Mathematics and Statistics Department Faculty
Publication Series

Mathematics and Statistics

2016

Discrete Solitons and Vortices in Anisotropic Hexagonal and Honeycomb Lattices

Q E. Hoq
Western New England University

Panayotis G. Kevrekidis
University of Massachusetts Amherst, kevrekid@math.umass.edu

A R. Bishop
Los Alamos National Laboratory

Discrete Solitons and Vortices in Anisotropic Hexagonal and Honeycomb Lattices

Q.E. Hoq

Department of Mathematics, Western New England University, Springfield, MA, 01119, USA

P.G. Kevrekidis[*]

Department of Mathematics and Statistics, University of Massachusetts, Amherst, Massachusetts 01003-4515 USA and
Center for Nonlinear Studies and Theoretical Division,
Los Alamos National Laboratory, Los Alamos, NM 87544

A.R. Bishop

Center for Nonlinear Studies and Theoretical Division,
Los Alamos National Laboratory, Los Alamos, NM 87544

In the present work, we consider the self-focusing discrete nonlinear Schrödinger equation on hexagonal and honeycomb lattice geometries. Our emphasis is on the study of the effects of anisotropy, motivated by the tunability afforded in recent optical and atomic physics experiments. We find that important classes of solutions, such as the so-called discrete vortices, undergo destabilizing bifurcations as the relevant anisotropy control parameter is varied. We quantify these bifurcations by means of explicit analytical calculations of the solutions, as well as of their spectral linearization eigenvalues. Finally, we corroborate the relevant stability picture through direct numerical computations. In the latter, we observe the prototypical manifestation of these instabilities to be the spontaneous rearrangement of the solution, for larger values of the coupling, into localized waveforms typically centered over fewer sites than the original unstable structure. For weak coupling, the instability appears to result in a robust breathing of the relevant waveforms.

I. INTRODUCTION

In both optical media [1] and atomic systems, such as Bose-Einstein condensates (BECs) [2], in the past two decades there has been a tremendous amount of effort focused on understanding the implications of periodic lattices. In the former case, both the realms of optical waveguides [3] and of photorefractive crystals [4] have played crucial roles towards the analysis and experimental realization of states such as discrete solitons, and vortices, as well as of more complex waveforms, including ring structures, necklaces, gap solitons and many others. In atomic BECs, on the other hand, the emphasis has not only been on corresponding matter waves [5], but also on quantum phenomena beyond the realm of mean-field models [6].

In recent years, the emphasis has somewhat shifted from the consideration of the more customary square lattices to the examination of lattices of hexagonal or honeycomb form. There, a source of emphasis has again been localization and self-trapping in the form of solitonic and vortical structures [7–9], but also other aspects have been studied including, e.g., Bloch states [10]. A significant fraction of the focus has been on the emulation by these optical systems of "photonic graphene", leading to numerous remarkable features, including the creation, destruction and experimental observation of topologically protected, so-called, edge states [11, 12], and also the emergence of pseudospin and angular momentum [13]. In the atomic realm too, considerably tunable and flexible optical lattices of both a hexagonal and honeycomb form have been produced for single [14] and multi-species [15] experiments. While much of the interest in this context lies within quantum mechanical transitions, such as the superfluid-insulator transition [6], the atoms can, very controllably, be considered in the superfluid regime where a mean-field description paralleling the optical one is suitable. As an aside, it is relevant to mention that more complex lattice structures including e.g. Kagomé lattices are also a subject of ongoing consideration [16, 17] and are within the realm of experimental possibility in both settings.

At the mathematical level, there exists a prototypical model that combines the suitable lattice geometry, the discreteness and the nonlinearity. As a result, it captures the principal features of the experimental observations, at least as regards the emerging coherent structures. This model is the so-called discrete nonlinear Schrödinger (DNLS) equation, which has been a subject of intense theoretical and numerical investigation [18]. Our aim in the present work is to utilize this DNLS model in order to capture the impact of anisotropy on the hexagonal and honeycomb

[*]Electronic address: kevrekid@math.umass.edu

lattices. This is in part motivated by the studies in optical photorefractive systems such as the work of [8] where both unstretched and stretched lattices were used and in both cases the coupling was anisotropic (varying in one direction between 20% and 80% of the coupling in the other directions). Such a systematic study is also motivated by the atomic realm of, e.g., [14], where the full control of the optical beam intensities, wavenumbers and phases that create the lattice trapping the atoms can straightforwardly be used to produce different types of lattices (e.g. both hexagonal and honeycomb) and different anisotropies.

Our aim here is to provide a systematic analysis of the different types of solutions that are possible in the anisotropic system. Starting from the isotropic two-dimensional limit, we vary the strength of the interaction along a particular direction. Progressively this leads from a two-dimensional configuration, e.g. in the honeycomb case, to an uncoupled set of quasi-one-dimensional configurations. As a result, we can appreciate that numerous states among those that exist in the two-dimensional (2d) setting should disappear at a suitable critical point as we approach the 1d regime. For instance, the discrete vortices belong to this category, as there are no solutions with nontrivial vorticity in one-dimensional DNLS lattices [18, 19]. Here, we intend to provide a quantification of the relevant solutions, as well as to provide a road map for their dynamical destabilization by evaluating their dominant linearization eigenvalues. Both of these steps are performed analytically (to leading order) permitting a complete characterization of the bifurcation events/destabilization or disappearance of different branches of solutions. This is done for the prototypical unit cell of each lattice i.e., for a triangular cell within the hexagonal lattice and a hexagonal cell within the honeycomb lattice, although it can be straightforwardly generalized to other cases. Once the existence, stability and bifurcations of the relevant solutions are determined, then their potential instabilities (and spectral properties) are also explored numerically. Finally, these findings are corroborated by direct numerical computations illustrating the tendency of the (unstable) dynamics towards (typically) fewer sites than the original structure. In the case of the 3-site cell in the hexagonal lattice, we observe a tendency of the dynamics towards the ground (single-site) state of the model for stronger couplings, or towards robust breathing excitations in the case of weaker couplings. In the case of the 6-site cell of the honeycomb lattice, even for stronger couplings, multi-site excitations (of different types – see details below) were typically found to persist over the evolution scales of dynamical propagation considered here.

Our presentation is structured as follows. In section II, we present our systematic analytical findings regarding the existence and stability of solutions for each of the lattices in their respective unit cells. Then in section III, we present the corresponding numerical findings, as well as examine, the fate of dynamically unstable solutions. Finally, in section IV, we summarize our results and present some challenges for future studies.

II. THEORETICAL ANALYSIS

To study the two geometries of interest, we consider the following discrete nonlinear Schrödinger equation

$$i\frac{du_{m,n}}{dz} = -\varepsilon\Delta_2 u_{m,n} - |u_{m,n}|^2 u_{m,n} \tag{1}$$

with the two-dimensional anisotropic discrete Laplacian

$$\Delta_2 u_{m,n} = \sum_{m',n'\in N_1} u_{m',n'} + \sum_{m'',n''\in N_2} \delta u_{m'',n''} - \frac{|N|}{3}(2+\delta)u_{m,n}. \tag{2}$$

Here, the constant ε denotes the strength of the linear coupling between nearest neighbor sites in the isotropic case and the anisotropy is controlled by the parameter δ ($0 \leq \delta \leq 1$). Since both of the grids of interest are rotationally invariant, hence there is a freedom in selecting the direction of the anisotropy. A value of $\delta = 1$ yields the isotropic lattice with a uniform nearest neighbor coupling of ε, whereas $\delta = 0$ completely decouples sites in the direction parallel to a particular lattice direction, chosen without loss of generality. Physically, the field $u_{m,n}$ represents (in our optical example) the envelope of the electric field in the waveguide, while in that case z is the propagation coordinate. For BECs, the field represents the atomic wavefunction in the corresponding well of the optical lattice, while z in that realization is replaced by the time t. The summations are over disjoint subsets, N_1 and N_2, of the set $N = N_1 \cup N_2$ of nearest neighbors where $|N| = 6$ for the hexagonal lattice and $|N| = 3$ for the honeycomb lattice. The set N_2 is the set of nearest neighbors joined to $u_{m,n}$ by the (anisotropic) coupling, $\delta\varepsilon$, while the remaining nearest neighbors belong to the set N_1 and have a coupling of ε to $u_{m,n}$. Note that in the case $\delta = 0$, the hexagonal grid becomes the usual rectangular grid, while the honeycomb grid becomes a parallel set of one-dimensional grids with (in both geometries) a nearest neighbor coupling of ε.

We are interested in stationary solutions of the form $u_{m,n} = \exp(i\Lambda z)v_{m,n}$, where Λ is the propagation constant in optics or the chemical potential in BECs. Then, $v_{m,n}$ satisfies the steady-state equation

$$\Lambda v_{m,n} = \varepsilon\Delta_2 v_{m,n} + |v_{m,n}|^2 v_{m,n}. \tag{3}$$

In the anticontinuum (AC) limit of uncoupled sites [20], (i.e. when $\varepsilon \to 0$), the solutions of Eq. (3) are $v_{m,n} = 0$ and $v_{m,n} = \sqrt{\Lambda} \exp(i\theta_{m,n})$. Thus, at the AC limit, explicit solutions of the form $u_k = \sqrt{\Lambda} \exp(i\theta_k) \exp(i\Lambda z)$ can be found over contours M of the uncoupled lattice points for arbitrary $\theta_k \in [0, 2\pi)$, where the nodes are indexed by k. For the current work, in the hexagonal lattice, k will index the sites along a three-site one-dimensional closed contour ($|M| = 3$), while in the honeycomb lattice, k will index the sites along a six-site one-dimensional closed contour ($|M| = 6$), i.e., we will consider the principal cells of the respective lattices. Without loss of generality, we set $\Lambda = 1$.

Following an analysis similar to that of [19, 21], we then find that the necessary (leading order) conditions for solutions over a discrete contour to persist for $\varepsilon > 0$ are given by

$$F_k = \delta_{k,k-1} \sin(\theta_k - \theta_{k-1}) + \delta_{k,k+1} \sin(\theta_k - \theta_{k+1}) = 0, \tag{4}$$

where we have the periodic condition $\theta_{k+|M|} = \theta_k$ for $k = 1, ..., |M|$, and the coefficients $\delta_{k,k-1}$ and $\delta_{k,k+1}$, provide the lattice anisotropy as defined by:

$$\delta_{k,l} = \begin{cases} \delta, & \text{if the segment of } M \text{ joining adjacent nodes } k \text{ and } l \text{ is parallel to the anisotropic direction} \\ 1, & \text{if the segment of } M \text{ joining adjacent nodes } k \text{ and } l \text{ is not parallel to the anisotropic direction.} \end{cases} \tag{5}$$

We will study the behavior of some solutions of the variety described above in both the hexagonal and honeycomb lattices when the "background" coupling, ε, is fixed at a small value and the anisotropy is switched on (i.e. $\delta < 1$). We will see that the anisotropy may stabilize or destabilize some solutions via, typically, pitchfork (i.e., symmetry breaking) bifurcations. Theoretically we will find that in the weak coupling limit, this transition from stability to instability, or vice-versa, occurs when the solution collides with another solution at $\delta = 0.5$ which then persists as the lattice becomes more anisotropic, until there is a complete decoupling in the prescribed direction.

Again, adapting the results of [19, 21] (see also the exposition of [18]), the stability of lattice excitations can be determined (to leading order) from the eigenvalues γ_k of the $|M| \times |M|$ Jacobian matrix of the form

$$\partial F_k/\partial \theta_l = \begin{cases} \delta_{k,k-1} \cos(\theta_k - \theta_{k-1}) + \delta_{k,k+1} \cos(\theta_k - \theta_{k+1}), & k = l \\ -\delta_{k,l} \cos(\theta_k - \theta_l), & k = l \pm 1 \\ 0, & |l - k| \geq 2. \end{cases} \tag{6}$$

When the excited nodes in the lattice are adjacent, the (near zero) stability eigenvalues λ_k of the full problem are given by $\lambda_k = \pm\sqrt{2\gamma_k \varepsilon}$ [19, 21]. We now examine some explicit examples of this general theoretical formulation of the anisotropic DNLS problem.

A. Hexagonal Lattice

In this subsection, we will analytically track the effects of anisotropy on the stability of various three-site configurations in the hexagonal lattice and make predictions about what the original configurations in the isotropic lattice transform into. The notation $[a, b, c]$ is employed to describe the three-site contour with phases a, b and c at the nodes (while a corresponding notation will be used for six-site contours). The contours we discuss here are: (1) $[0, 2\pi/3, 4\pi/3]$ (charge one vortex), (2) $[0, \pi, 0]$, and (3) $[0, 0, 0]$. These are the principal (up to trivial transformations of phase) 3-site solutions of the hexagonal lattice cell.

(1) We begin with the three-site single charged vortex ($\theta_1 = 0, |\Delta\theta| = \frac{2\pi}{3}$). From Eq. (4) with $|M| = 3$ and with the anisotropy lying between the sites with phases θ_1 and θ_3, we obtain the following relationship between the phases:

$$\begin{aligned} \theta_3 &= \theta_1 + 2\arccos\left(-\frac{1}{2\delta}\right) & 0.5 \leq \delta \leq 1 \\ \theta_2 &= \frac{\theta_1 + \theta_3}{2} & (\text{mod } 2\pi). \end{aligned} \tag{7}$$

Using this phase profile in Eq. (6), the Jacobian matrix becomes

$$\mathbf{J} = \begin{pmatrix} \cos\left(\frac{\theta_1-\theta_3}{2}\right) + \delta\cos\left(\theta_1 - \theta_3\right) & -\cos\left(\frac{\theta_1-\theta_3}{2}\right) & -\delta\cos\left(\theta_1 - \theta_3\right) \\ -\cos\left(\frac{\theta_1-\theta_3}{2}\right) & 2\cos\left(\frac{\theta_1-\theta_3}{2}\right) & -\cos\left(\frac{\theta_1-\theta_3}{2}\right) \\ -\delta\cos\left(\theta_1 - \theta_3\right) & -\cos\left(\frac{\theta_1-\theta_3}{2}\right) & \cos\left(\frac{\theta_1-\theta_3}{2}\right) + \delta\cos\left(\theta_1 - \theta_3\right) \end{pmatrix}. \tag{8}$$

Thus, for $0.5 \leq \delta \leq 1$ the eigenvalues γ_k are found to be $\gamma_1 = 0$, $\gamma_2 = \cos\left(\frac{\theta_1 - \theta_3}{2}\right) + 2\delta \cos(\theta_1 - \theta_3)$ and, $\gamma_3 = 3\cos\left(\frac{\theta_1 - \theta_3}{2}\right)$. In particular, for the hexagonal three-site charge-one vortex (which satifies Eq. (7)) the stability eigenvalues for $0.5 \leq \delta \leq 1$ are found to be $\lambda_1 = \{0, 0\}$, $\lambda_2 = \pm\sqrt{\frac{(4\delta^2 - 1)\varepsilon}{\delta}} i$, and $\lambda_3 = \pm\sqrt{\frac{3\varepsilon}{\delta}} i$. For this range of values of δ, all of the quantities in the radicals within the eigenvalue pairs remain nonnegative and, for sufficiently small ε, the pair λ_3 will not collide with the continuous spectrum. Hence, this vortex remains stable throughout this interval of anisotropy. Note that the only eigenvalue pair that moves along the imaginary axis towards the origin of the spectral plane and thus has the potential to bring about instability when $0 \leq \delta < 0.5$ is $\lambda_2 = \pm\sqrt{\frac{(4\delta^2 - 1)\varepsilon}{\delta}} i$. As the above solution of Eq. (7) cannot be continued below $\delta = 0.5$, additional analysis is needed to reveal the outcome for a further increase in anisotropy, i.e. for $0 \leq \delta < 0.5$.

From Eq. (7), we can also determine the theoretical predictions for the changes in the relative phases (mod 2π) as a function of δ for $0.5 \leq \delta \leq 1$:

$$|\theta_2 - \theta_1| = |\theta_3 - \theta_2| = \frac{1}{2}|\theta_1 - \theta_3| = \arccos\left(-\frac{1}{2\delta}\right). \tag{9}$$

In the isotropic case (i.e. when $\delta = 1$) for all the relative phases we have $|\Delta\theta| = \frac{2\pi}{3}$. As the anisotropy increases, reaching $\delta \to 0.5$, we find that $|\theta_2 - \theta_1| \to \pi$, $|\theta_3 - \theta_2| \to \pi$, and $|\theta_1 - \theta_3| \to 0$. Thus, at this critical point, the single-charge vortex $[0, \frac{2\pi}{3}, \frac{4\pi}{3}]$, merges with the configuration $[\theta_1, \theta_1 + \pi, \theta_1 + 2\pi] = [\theta_1, \theta_1 + \pi, \theta_1](\text{mod } 2\pi)$ i.e., with the $[0, \pi, 0]$ state. Exploring the latter state and its stability for $0 \leq \delta \leq 0.5$ (or, in fact, for any δ since the solution persists $\forall \delta$), the corresponding Jacobian of Eq. (6) assumes the form

$$\mathbf{J} = \begin{pmatrix} -1 + \delta & 1 & -\delta \\ 1 & -2 & 1 \\ -\delta & 1 & -1 + \delta \end{pmatrix}. \tag{10}$$

The associated stability eigenvalues become $\lambda_1 = \{0, 0\}$, $\lambda_2 = \pm\sqrt{6\varepsilon} i$, and $\lambda_3 = \pm\sqrt{2(1 - 2\delta)\varepsilon} i$. Of particular note is the eigenvalue pair λ_3 which remains imaginary for $0 \leq \delta < 0.5$. Thus, this solution is stable for $0 \leq \delta \leq 0.5$, but it destabilizes through a pitchfork bifurcation, giving rise to the discrete vortex (inheriting its stability) for $\delta > 0.5$.

(2) Given our analysis of the $[0, \pi, 0]$ state above in connection with the vortex bifurcation, we will not discuss further here the case with anisotropy between sites with phase 0.

For the $[0, \pi, 0]$ state with anisotropy between the site with phase π and one of the 0 phase sites, the Jacobian matrix is

$$\mathbf{J} = \begin{pmatrix} 0 & 1 & -1 \\ 1 & -1 - \delta & \delta \\ -1 & \delta & 1 - \delta \end{pmatrix} \tag{11}$$

from which we find the stability eigenvalues to be $\lambda_1 = \{0, 0\}$ and $\lambda_2 = \pm\sqrt{2(-\delta + \sqrt{\delta^2 + 3})\varepsilon}$, $\lambda_3 = \pm\sqrt{2(\delta + \sqrt{\delta^2 + 3})\varepsilon} i$. The eigenvalue pair λ_2 remains real valued throughout the change of δ and thus we see that this solution remains unstable.

(3) In the isotropic lattice the stability eigenvalues of the hexagonal $[0, 0, 0]$ configuration are found to be $\lambda_1 = \{0, 0\}$, $\lambda_2 = \pm\sqrt{6\varepsilon}$, and $\lambda_3 = \pm\sqrt{6\varepsilon}$. Not surprisingly, due to the adjacent in-phase sites, this is unstable. In the case of $\delta \neq 1$, this instability persists. From our above analysis, the relevant eigenvalues can be directly found to be $\lambda_1 = \{0, 0\}$, $\lambda_2 = \pm\sqrt{6\varepsilon}$, and $\lambda_3 = \pm\sqrt{2(2\delta + 1)\varepsilon}$. Despite the significant dependence of λ_2 on δ, we see that this configuration is indeed generically expected to be unstable.

B. Honeycomb Lattice

We now analytically examine the stability and transformation of solutions in the anisotropic honeycomb lattice and its six-site cell ($|M| = 6$). Similar to what was done for the hexagonal lattice, we will deduce relationships between the phases for a few prototypical configurations in the honeycomb lattice. In each solution, the anisotropy lies between the sites with phases θ_3 and θ_4 and also between sites with phases θ_6 and θ_1. The structures we will present here assume the following form in the isotropic limit of $\delta = 1$: (1) $[0, \frac{\pi}{3}, \frac{2\pi}{3}, \pi, \frac{4\pi}{3}, \frac{5\pi}{3}]$ (charge 1 vortex), (2) $[0, \frac{2\pi}{3}, \frac{4\pi}{3}, 2\pi, \frac{8\pi}{3}, \frac{10\pi}{3}]$ (charge 2 vortex), (3) $[0, \pi, 0, \pi, 0, \pi]$ (4) $[0, 0, 0, 0, 0, 0]$. While additional configurations are possible here (in particular

all combinations of 0 and π phase are possible within the 6 sites), these configurations are the most interesting ones and will provide a basic understanding of the stability properties of the anisotropic system.

(1) The honeycomb six-site charge 1 vortex ($\theta_1 = 0, |\Delta\theta| = \frac{\pi}{3}$) satisfies the following phase relationships which can be deduced from Eq.(4):

$$
\begin{aligned}
\theta_3 &= \theta_1 + 2\arccos\left(\frac{1}{2\delta}\right) & 0.5 \le \delta \le 1 \\
\theta_2 &= \frac{\theta_1 + \theta_3}{2} \\
\theta_4 &= \theta_1 + \pi \\
\theta_5 &= \frac{\theta_1 + \theta_3}{2} + \pi \\
\theta_6 &= \theta_3 + \pi & (\text{mod } 2\pi).
\end{aligned}
\tag{12}
$$

Using these results with the Jacobian matrix of Eq. (6), we find that the stability eigenvalues of the charge 1 vortex are $\lambda_1 = \{0,0\}$, $\lambda_2 = \pm\sqrt{\frac{\varepsilon}{\delta}}$, $\lambda_3 = \pm\sqrt{\frac{(4\delta^2-1)\varepsilon}{\delta}}$, $\lambda_4 = \pm\sqrt{\frac{3\varepsilon}{\delta}}$, and

$$
\lambda_{5,6} = \pm\sqrt{\left(\frac{1+4\delta^2}{2\delta} \pm \sqrt{-4 + \frac{21}{8\delta^2} + 9\cos(\alpha(\delta)\beta(\delta)) + 4\delta^2\cos(4\alpha(\delta)\beta(\delta)) + \left(\frac{16\delta^2-9}{2}\right)\cos^2(\alpha(\delta)) - 8\delta^2\cos^4(\alpha(\delta))}\right)\varepsilon}
$$

where $\alpha(\delta) = \theta_1 + \arccos\left(\frac{1}{2\delta}\right)$, $\beta(\delta) = \arccos\left(\frac{1}{2\delta}\right)$. It is clear that at least the eigenvalue pairs λ_1, λ_2, and λ_3 all remain real-valued as $\delta \to 0.5$ and hence the charge 1 vortex is unstable on the entire interval $0.5 \le \delta \le 1$.

The changes in the relative phases (mod 2π) as a function of δ for $0.5 \le \delta \le 1$ are given by:

$$
|\theta_2 - \theta_1| = |\theta_3 - \theta_2| = |\theta_5 - \theta_4| = |\theta_6 - \theta_5| = \arccos\left(\frac{1}{2\delta}\right)
$$

$$
|\theta_4 - \theta_3| = \pi - 2\arccos\left(\frac{1}{2\delta}\right)
$$

$$
|\theta_1 - \theta_6| = \pi + 2\arccos\left(\frac{1}{2\delta}\right).
$$

In the isotropic case ($\delta = 1$), all the relative phases satisfy $|\Delta\theta| = \frac{\pi}{3}$. But as $\delta \to 0.5$, we find that $|\theta_{i+1} - \theta_i| \to 0$ for $i = 1, 2, 4, 5$, while $|\theta_4 - \theta_3| \to \pi$ and, $|\theta_1 - \theta_6| \to \pi$. Also as $\delta \to 0.5$, from Eq.(12) we theoretically predict that the charge 1 vortex in the isotropic lattice merges at with $[\theta_1, \theta_1, \theta_1, \theta_1 + \pi, \theta_1 + \pi, \theta_1 + \pi]$ at $\delta = 0.5$. As was shown in more detail with the hexagonal three-site charge 1 vortex, the stability eigenvalues for the interval $0 \le \delta \le 0.5$ can be obtained and appear more simply as $\lambda_1 = \{0,0\}$, $\lambda_2 = \pm\sqrt{2\varepsilon}$, $\lambda_3 = \pm\sqrt{2(1-2\delta)\varepsilon}$, $\lambda_4 = \pm\sqrt{6\varepsilon}$ and, $\lambda_{5,6} = \pm\sqrt{(3 - 2\delta \pm \sqrt{4\delta^2 + 4\delta + 9})\varepsilon}$. Thus, we have instability throughout the change in the anisotropy. More generally, the established "rule of thumb" for self-focusing nonlinearities is that whenever sites of the same phase are adjacent to each other, the configuration will inherit an instability associated with a real eigenvalue pair. Hence, it is natural to expect, based on the structural form of the configuration $[\theta_1, \theta_1, \theta_1, \theta_1 + \pi, \theta_1 + \pi, \theta_1 + \pi]$, that it will be unstable for all values of δ. Nevertheless, one of its real pairs for $\delta < 0.5$ will become imaginary for $\delta > 0.5$, giving rise to an unstable daughter state, namely the single charge vortex solution.

(2) The honeycomb six-site charge-2 vortex ($\theta_1 = 0, \Delta\theta = \frac{2\pi}{3}$ for $\delta = 1$) satisfies

$$
\begin{aligned}
\theta_3 &= \theta_1 + 2\arccos\left(-\frac{1}{2\delta}\right) & 0.5 \le \delta \le 1 \\
\theta_2 &= \frac{\theta_1 + \theta_3}{2} \\
\theta_4 &= \theta_1 + 2\pi \\
\theta_5 &= \frac{\theta_1 + \theta_3}{2} + 2\pi \\
\theta_6 &= \theta_3 + 2\pi & (\text{mod } 4\pi)
\end{aligned}
\tag{13}
$$

and the stability eigenvalues for the charge 2 vortex are $\lambda_1 = \{0,0\}$, $\lambda_2 = \pm\sqrt{\frac{\varepsilon}{\delta}}i$, $\lambda_3 = \pm\sqrt{\frac{(4\delta^2-1)\varepsilon}{\delta}}i$, $\lambda_4 = \pm\sqrt{\frac{3\varepsilon}{\delta}}i$, and

$$
\lambda_{5,6} = \pm\sqrt{\left(\frac{1+4\delta^2}{2\delta} \pm \sqrt{-4 + \frac{21}{8\delta^2} + 9\cos(\alpha(-\delta)\beta(-\delta)) + 4\delta^2\cos(4\alpha(-\delta)\beta(-\delta)) + \left(\frac{16\delta^2-9}{2}\right)\cos^2(\alpha(-\delta)) - 8\delta^2\cos^4(\alpha(-\delta))}\right)\varepsilon}\,i,
$$

where as before $\alpha(\delta) = \theta_1 + \arccos\left(\frac{1}{2\delta}\right)$, $\beta(\delta) = \arccos\left(\frac{1}{2\delta}\right)$.

The changes in the relative phases as a function of δ for $0.5 \leq \delta \leq 1$ are given by:

$$|\theta_2 - \theta_1| = |\theta_3 - \theta_2| = |\theta_5 - \theta_4| = |\theta_6 - \theta_5| = \arccos\left(-\frac{1}{2\delta}\right)$$

$$|\theta_4 - \theta_3| = 2\pi - 2\arccos\left(-\frac{1}{2\delta}\right)$$

$$|\theta_1 - \theta_6| = 2\pi + 2\arccos\left(-\frac{1}{2\delta}\right).$$

In the isotropic honeycomb lattice ($\delta = 1$), all the relative phases satisfy $|\Delta\theta| = \frac{2\pi}{3}$. But as $\delta \to 0.5$, we find that $|\theta_{i+1} - \theta_i| \to \pi$ for $i = 1, 2, 4, 5$, while $|\theta_4 - \theta_3| \to 0$ and, $|\theta_1 - \theta_6| \to 0$. Also, as $\delta \to 0.5$, from Eq. (13) we theoretically predict that the charge 2 vortex in the isotropic lattice merges at $\delta = 0.5$ with $[\theta_1, \theta_1 + \pi, \theta_1 + 2\pi, \theta_1 + 2\pi, \theta_1 + 3\pi, \theta_1 + 4\pi] = [\theta_1, \theta_1 + \pi, \theta_1, \theta_1, \theta_1 + \pi, \theta_1]$ (mod 2π). The stability eigenvalues of the latter state for $0 \leq \delta \leq 0.5$ are $\lambda_1 = \{0, 0\}$, $\lambda_2 = \pm\sqrt{2\varepsilon}i$, $\lambda_3 = \pm\sqrt{2(1 - 2\delta)\varepsilon}i$, $\lambda_4 = \pm\sqrt{6\varepsilon}i$, $\lambda_5 = \pm\sqrt{(-3 + 2\delta - \sqrt{4\delta^2 + 4\delta + 9})\varepsilon} = \pm\sqrt{(3 - 2\delta + \sqrt{4\delta^2 + 4\delta + 9})\varepsilon}i$, $\lambda_6 = \pm\sqrt{(-3 + 2\delta + \sqrt{4\delta^2 + 4\delta + 9})\varepsilon}$. Note that λ_6 is real for $0 \leq \delta \leq 0.5$ and so it is expected that the stable vortex of the isotropic limit with $\delta = 1$ becomes unstable for some δ in $0.5 < \delta < 1$. As regards the state $[\theta_1, \theta_1 + \pi, \theta_1, \theta_1, \theta_1 + \pi, \theta_1]$ (mod 2π), the above analysis predicts that it also undergoes a supercritical pitchfork bifurcation giving rise to the charge 2 vortex which inherits its (in)stability properties and is eventually full stabilized for a larger value of δ in $0.5 < \delta < 1$. In fact, using the expression for λ_6 given above for the charge-2 vortex, we find that the relevant critical point is $\delta = 0.716$, which we will compare with our numerical computations in the following section.

(3) In a similar way to the analysis done above, the stability eigenvalues for the six-site configuration of alternating sites $[0, \pi, 0, \pi, 0, \pi]$ are found to be $\lambda_1 = \{0, 0\}$, $\lambda_2 = \pm\sqrt{6\varepsilon}i$, $\lambda_3 = \pm\sqrt{2\varepsilon}i$, $\lambda_4 = \pm\sqrt{2(2\delta + 1)\varepsilon}i$ $\lambda_{5,6} = \pm\sqrt{(3 + 2\delta \pm \sqrt{4\delta^2 - 4\delta + 9})\varepsilon}i$. The imaginary eigenvalues indicate that this configuration is stable both in the isotropic and anisotropic lattices.

(4) Finally the six-site configuration of in-phase sites $[0, 0, 0, 0, 0, 0]$ has the stability eigenvalues $\lambda_1 = \{0, 0\}$, $\lambda_2 = \pm\sqrt{6\varepsilon}$, $\lambda_3 = \pm\sqrt{2\varepsilon}$, $\lambda_4 = \pm\sqrt{2(2\delta + 1)\varepsilon}$ $\lambda_{5,6} = \pm\sqrt{(3 + 2\delta \pm \sqrt{4\delta^2 - 4\delta + 9})\varepsilon}$. Given the presence of real eigenvalues, this configuration is unstable. Similarly to what we saw previously for the 3-site configuration in the hexagonal lattice, the presence of adjacent in-phase sites is detrimental to the stability of this configuration for arbitrary values of δ. Hence, no stabilization of the relevant state is anticipated, independently of the particular value of the anisotropy parameter δ.

III. NUMERICAL RESULTS

In this section we present our numerical findings for the various configurations in the hexagonal and honeycomb lattices and compare these results with the theoretical findings from the previous section. In all cases, we use a Newton-Raphson fixed point iteration to identify the full numerical solution over the two-dimensional lattices. This process is initiated at the AC limit and continued to a small coupling while maintaining $\delta = 1$ to yield the isotropic case. In most of the examples we consider, the Newton-Raphson interation is continued to $\varepsilon = 0.01$, but a few cases will also be examined where the fixed point iteration is continued to a higher value of ε. The anisotropy (as described in a previous section) is introduced by letting δ deviate from the isotropic unity value and performing a continuation in decreasing values of the parameter towards $\delta \to 0$. We present figures that show each configuration, along with its phase portrait and spectral plane at some δ before and after the relevant bifurcation points, comparing the latter with our theoretical predictions. It is generally found that for values of the coupling, ε, near the AC limit the theoretical predictions match the numerical results very well.

The theoretical predictions of the linearization eigenvalues will be compared to the numerical results for the linear stability of the stationary solution $v_{m,n} \exp(iz)$ by using the ansatz

$$u_{m,n} = e^{iz}\left[v_{m,n} + \gamma(a_{m,n}e^{\lambda z} + b^*_{m,n}e^{\lambda^* z})\right]. \tag{14}$$

The eigenvalue problem that follows is then solved for the eigenvalues λ and eigenvectors $(a_{m,n}, b_{m,n})^T$. The asterisk denotes complex conjugate while T denotes transpose.

A. Hexagonal Lattice

(1) We start with the hexagonal lattice and begin by presenting the results of the continuation for the three site charge 1 vortex with coupling $\varepsilon = 0.01$ (see Fig. 1). Initially, at $\delta = 1$, the configuration has phases $\theta_1 = 0, \theta_2 = 2\pi/3, \theta_3 = 4\pi/3$, with the anisotropy to be activated between the sites with phases θ_1 and θ_3. The top row of Fig. 1 shows the square modulus of the field ($|u_{n,m}|^2$) for the vortex at $\delta = 0.8$ (left panel) and at $\delta = 0$ (right panel), while the second and third rows show, respectively, the corresponding phase portraits and spectral planes. The left panel of the fourth row shows the change in the relative phases ($|\Delta\theta|$) and the right panel traces the linear stability eigenvalues with the change in anisotropy. In both images the theory (dash-dot lines) compares extremely well with the numerical (solid lines) results, over the entire interval of continuation of the anisotropy parameter δ. In the case of $\delta \to 0$ it is evident that the configuration has changed its character into a $[0, \pi, 0]$ configuration, as theoretically predicted. The relative phase and eigenvalue predictions of the bottom row indeed confirm that the pitchfork bifurcation takes place at $\delta = 0.5$ and leads to a collision with the configuration $[-\pi/3, 2\pi/3, -\pi/3]$ at $\delta = 0.5$ (which as theoretically predicted has the form $[\theta_1, \theta_1 + \pi, \theta_1]$, i.e., up to a trivial phase is a $[0, \pi, 0]$ configuration). We note in passing that we have also examined the relevant continuation and bifurcation for other values of ε (such as $\varepsilon = 0.05$), finding similar qualitative results (although quantitative details, such as the critical value of δ do change).

(2) The hexagonal $[0, \pi, 0]$ configuration can be seen in Figs. 2 and 3. In the isotropic lattice of $\varepsilon = 0.01$ this solution is unstable. However stability can be achieved if the anisotropy is activated between the the two nodes with phase 0, while any other placement maintains the instability. This is because if the nodes with the same phase are connected at the $\delta \to 0$ limit (where we can think of the three nodes as effectively being on a straight line), then, as discussed above, the instability due to a real eigenvalue pair will be maintained. In the case where a stabilization effect is observed (in Fig. 2) $[0, \pi, 0]$, as δ decreases, a weakened bond between the 0 phase nodes results and eventually an effective $[0, \pi, 0]$ state along a line is effectively obtained which is well known to be stable, as a one-dimensional configuration, for small ε [19]. The change of stability occurs at $\delta = 0.49$, in excellent agreement with the theoretical prediction of $\delta = 0.5$. On the other hand, an anisotropic weakening of the bond between the site with phase π and either of the 0 phase sites does not bring about stability and eventually just yields an unstable waveform (along an effective line) $[0, 0, \pi]$, which has been demonstrated to be unstable in 1d settings [19].

(3) The hexagonal $[0, 0, 0]$ configuration (Fig. 4) is, not surprisingly, unstable in the isotropic lattice ($\varepsilon = 0.01$) due to the adjacent in-phase sites and, in full accordance with our theoretical predictions, this remains unstable as $\delta \to 0$.

B. Honeycomb Lattice

We now discuss the effects of anisotropy in the honeycomb lattice. For the case of the six-site charge 1 vortex (see Fig. 5), we again see a very good comparison between the numerical results and the theory. The unstable charge 1 vortex remains unstable throughout the anisotropic variation of δ in the interval $[0, 1)$. At about $\delta = 0.70$ one of the real eigenvalue pairs $\lambda_{5,6}$ collides with the origin of the spectral plane and becomes purely imaginary. At $\delta = 0.5$ the pair which was theoretically predicted to be $\lambda_3 = \pm\sqrt{\frac{(4\delta^2-1)\varepsilon}{\delta}}$ collides with the pair λ_1, giving rise to the bifurcation that was theoretically predicted to arise at this critical point. Indeed this bifurcation transforms the vortex for $\delta < 0.5$ into the unstable $[\pi/3, \pi/3, \pi/3, 2\pi/3, 2\pi/3, 2\pi/3]$ honeycomb configuration (i.e., a $[0, 0, 0, \pi, \pi, \pi]$ state up to a trivial phase shift, as discussed in section II).

The stable honeycomb charge 2 vortex (shown in Fig. 6) becomes unstable at approximately $\delta = 0.70$, in very good agreement with the theoretical prediction of $\delta = 0.716$; cf. the relevant discussion in section II. The instability arises due to a pair of eigenvalues from $\lambda_{5,6}$ becoming real-valued. Subsequently, as theoretically predicted, for $\delta = 0.5$, a pitchfork bifurcation eventually transforms the vortex into the state $[-\pi/3, 2\pi/3, -\pi/3, -\pi/3, 2\pi/3, -\pi/3]$, (i.e., a $[0, \pi, 0, 0, \pi, 0]$ state up to a trivial phase shift). The latter configuration has the same stability characteristics for $\delta < 0.5$ that the vortex state possesses in the vicinity of $\delta > 0.5$. Therefore, it possesses a single real eigenvalue pair as confirmed in the right panels of Fig. 6. Naturally, for $\delta > 0.5$, this $[0, \pi, 0, 0, \pi, 0]$ persists but acquires a second real pair as a result of the supercritical pitchfork bifurcation.

In addition to these vortex configurations, in Figs. 7 and 8, we also examined the states with phase configurations: $[0, \pi, 0, \pi, 0, \pi]$ and $[0, 0, 0, 0, 0, 0]$, respectively. The former, as expected (for this small ε and given its alternating phase structure) is found to be linearly stable for all the considered values of δ, while the latter is found to be highly unstable bearing 5 distinct real eigenvalue pairs (as anticipated due to the presence of sites of the same phase adjacent to each other).

IV. DYNAMICS

In this section we numerically examine the nonlinear dynamics of the unstable solutions discussed in the previous sections. Each unstable solution is perturbed slightly in the direction of the eigenvector corresponding to the most unstable eigenvalue, in order to seed the relevant instabilities. A fourth order (explicit) Runge-Kutta algorithm (RK4) has been used in order to obtain the relevant dynamical evolution results. It is observed that the coupling significantly controls the nature of the dynamical evolution. This is natural since a larger coupling allows nearest neighbors to interact more strongly. In the hexagonal lattice, we show the evolution at a fixed background coupling of $\varepsilon = 0.01$ and also $\varepsilon = 0.2$. In all cases, the smaller coupling leads to a robust (multi-site) breather form, while the larger coupling produces a single robust site. For the honeycomb lattice case, a coupling of $\varepsilon = 0.2$ is used. All the unstable honeycomb six-site solutions evolve into multi-site breathers (where the number of sites participating with a large norm in the final configuration varies from case to case; see below). In either lattice we hold the anisotropy fixed at $\delta = 0.8$ for instabilities above the critical threshold of $\delta = 0.5$, and to $\delta = 0.2$ if the instability occurs below $\delta = 0.5$. The one exception is for the charge 2 vortex where we present the dynamics at $\delta = 0.6$ (instead of $\delta = 0.8$), i.e. after the onset of instability but before the critical transformation point of that state.

A. Hexagonal Lattice

The solutions found to be unstable in the hexagonal geometry are (1) $[0, \pi, 0]$ with the anisotropy between the 0 phase sites when $\delta > 0.5$ (due to the bifurcation of the vortex state), (2) $[0, \pi, 0]$ with the anisotropy between the site with phase π and one of the sites with phase 0, (3) $[0, 0, 0]$.

(1) Figures 9 and 10 exhibit the dynamics in the anisotropic hexagonal lattice for $[0, \pi, 0]$ when the anisotropy is prescribed to be between the sites with phase 0 with $\varepsilon = 0.01$ and $\varepsilon = 0.2$ respectively. In both instances, we use $\delta = 0.8$. In the case of the weaker coupling, the propagating solution shows oscillatory (i.e., breathing) behavior. In fact, we observe similar features for the weak coupling case of $\varepsilon = 0.01$ for all the unstable solutions studied here. For the larger coupling of $\varepsilon = 0.2$ in Fig. 10 we see a clear destruction of the original waveform and an emergence of a single surviving site that persists. It may be interesting in future work to explore the transition regime between weak and strong coupling and the associated implications for the nature of the resulting states.

(2) The $[0, \pi, 0]$ solution with anisotropy between the site with phase π and one with 0 is unstable for all values of δ, as discussed previously. As in the previous example, for $\varepsilon = 0.01$ the dynamics shows an oscillatory movement during propagation. However, when the coupling is set to $\varepsilon = 0.2$, destruction of the wave is observed with, as before, a single site persisting for long times. Given the similarity of these findings to those of Figs. 9 and 10 we omit them here.

(3) Finally the evolution of the form $[0, 0, 0]$ is seen in Figs. 11 and 12. The solution is unstable for all $0 \le \delta \le 1$. We see essentially the same qualitative behavior as for the previous two cases, as regards the asymptotic fate of the unstable waveforms. We have also checked that this phenomenology arises for different values of δ, such as $\delta = 0.2$ (results not shown here).

B. Honeycomb Lattice

Finally, we now turn to case examples of the dynamical evolution on the honeycomb lattice. The unstable solutions that we study in this case are: (1) the charge one vortex, (2) the charge-2 vortex for $\delta < 0.716$ (below 0.5, recall that this states morphs into an unstable $[0, 0 + \pi, 0, 0, 0 + \pi, 0]$ state), (3) the in-phase solution $[0, 0, 0, 0, 0, 0]$. Given that the results for weak coupling are similarly (breathing) as in the previous subsection, we focus on the case of the larger coupling $\varepsilon = 0.2$.

(1) The charge 1 vortex is unstable for the full range of the anisotropy considered herein. In Fig. 13, we explore its unstable dynamics for a coupling strength of $\varepsilon = 0.2$ and $\delta = 0.8$; similar results have also been found for other values of δ, as e.g. in Fig. 14 for $\delta = 0.2$. The dynamics yields a multi-site excitation, but with a repartitioning of the relevant intensity so that some sites are dominant in amplitude in comparison to others.

(2) In Fig. 15 we see the dynamics of the charge 2 vortex after the onset of instability, at $\delta = 0.6$. The result is a six site breathing structure with a complex norm redistribution. In Fig. 16, we show the dynamics of the unstable solution of the form $[0, 0 + \pi, 0, 0, 0 + \pi, 0]$, resulting from the pitchfork bifurcation of the charge-2 vortex for the case of $\delta < 0.5$. Specifically, in this example for $\delta = 0.2$, a breathing six-site excitation appears to persist.

(3) Finally, the dynamical evolution of the unstable state $[0, 0, 0, 0, 0, 0]$ for $\delta = 0.8$ in Fig. 17 (but also for other values of δ) illustrates the dynamical tendency of this state towards configurations with fewer –arguably two, at the final evolution snapshot shown– dominant (in amplitude) sites.

V.   CONCLUSIONS AND FUTURE CHALLENGES

In summary, in the present work, we have explored the existence, stability and dynamics of localized states (focusing on multi-site solitonic and vortex states) in hexagonal and honeycomb lattices. We considered the prototypical unit cells in each case, namely a 3-site one in the hexagonal case and a 6-site one in the honeycomb case. Analytical considerations in the vicinity of the anti-continuum limit permitted us to identify the states in the presence of anisotropy in an approximate analytical form and gave us the ability to consider the linear (spectral) stability eigenvalues and obtain approximate analytical expressions for them. These results allowed us to elucidate the pitchfork bifurcations that lead to the disappearance of states such as vortices (and the destabilization of other solitonic states) as the path from more effectively one-dimensional to effectively two-dimensional configurations is traversed. These existence and stability findings were also found to be in good agreement with detailed numerical continuations (over the anisotropy parameter), at least for small values of the coupling. Finally, the dynamics of the relevant structures were examined, allowing us to identify some gross features, including the breathing nature of the instability for very weak ε and the potential for stronger localization (typically to a smaller number of sites) ensuing as a result of instability for stronger ε.

A significant number of possibilities emerge from the present work for future explorations. On the one hand, it would be relevant and interesting to examine in more detail the dynamical evolution scenarios of the model, and to provide a more systematic characterization of the propagation outcomes for cases of both weaker and stronger coupling. On the other hand, extending similar studies to the case of Kagomé lattices and their flat bands, identifying the spectral properties not only of the solitons/vortices [16] but also of the compactly supported structures [17] identified therein would be a timely theme. Finally, extending such considerations to three-dimensional lattices of different types would also pose significant new challenges and can be expected to feature intriguing bifurcation phenomena and states of interest. Efforts along these directions are presently underway and will be reported in future publications.
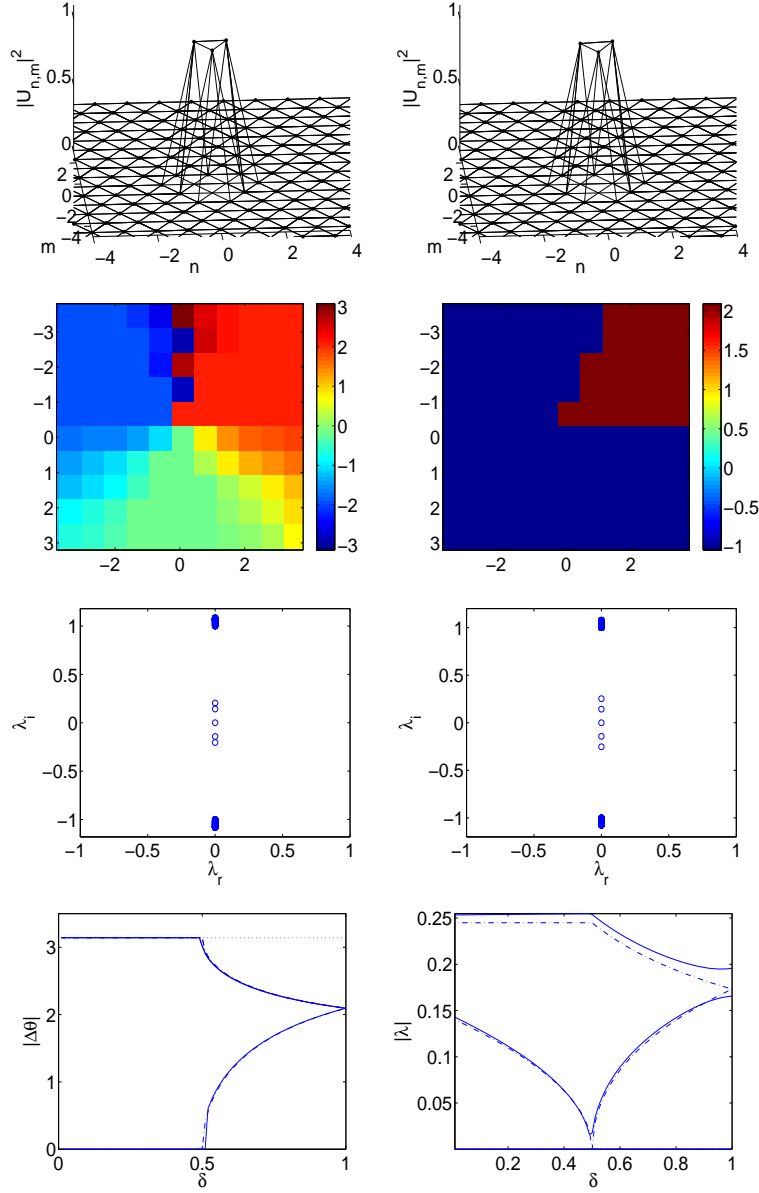
FIG. 1: Hexagonal three-site charge 1 vortex i.e. the hexagonal $[0, 2\pi/3, 4\pi/3]$ configuration (at $\varepsilon = 0.01$). The anisotropy here is activated between the sites with (initial) phases 0 and $4\pi/3$ when $\delta = 1$. The top row displays the modulus squared of the configuration corresponding to anisotropic parameter $\delta = 0.8$ (left panel) and $\delta = 0$ (right panel). The second row shows the phase portraits and the third row shows the spectral plane for the same values of the anisotropy, $\delta = 0.8$ (left), and $\delta = 0$ (right). In the fourth row, the left panel shows the comparison between the theoretical (dash-dot lines) and numerical (solid lines) changes in the relative phases. The charge 1 vortex collides at $\delta = 0.5$ with the stable (for lower values of δ) hexagonal $[-\pi/3, 2\pi/3, -\pi/3]$ configuration. When $\delta = 0$ this is equivalent to the $[-\pi/3, 2\pi/3, -\pi/3]$ configuration, i.e., effectively a $[0, \pi, 0]$ configuration. The fourth row right panel shows a theoretical (dash-dot lines) versus numerical (solid lines) comparison of the stability eigenvalues for $0 \le \delta \le 1$.
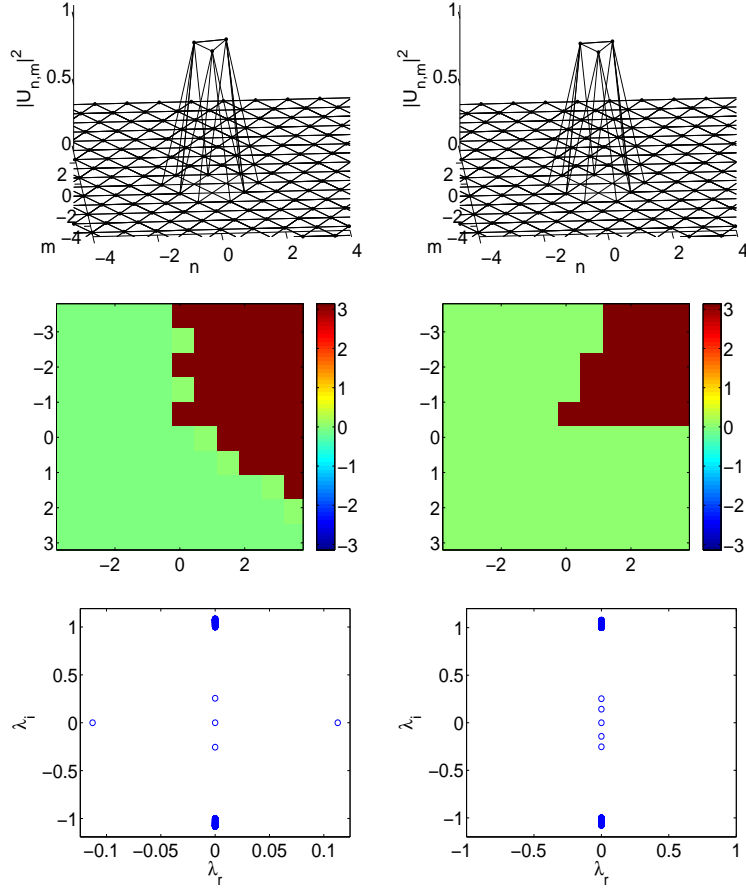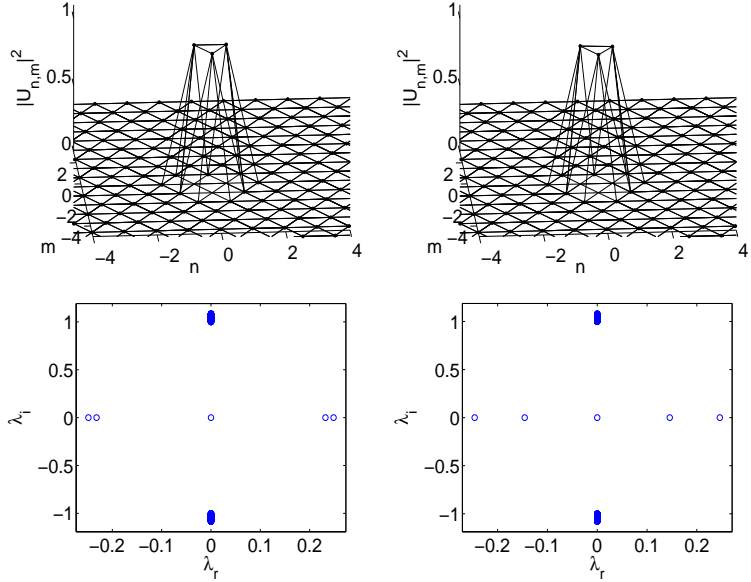
FIG. 2: Hexagonal three-site $[0, \pi, 0]$ configuration ($\varepsilon = 0.01$). The top row displays the modulus squared of the field at $\delta = 0.8$ (left column) and $\delta = 0$ (right column). The second row shows the corresponding phase portraits while the third row displays the respective spectral planes. In this case, the anisotropy is invoked between the two nodes with phase 0. Hence, as discussed in the text a stabilization is observed for $\delta < 0.5$.
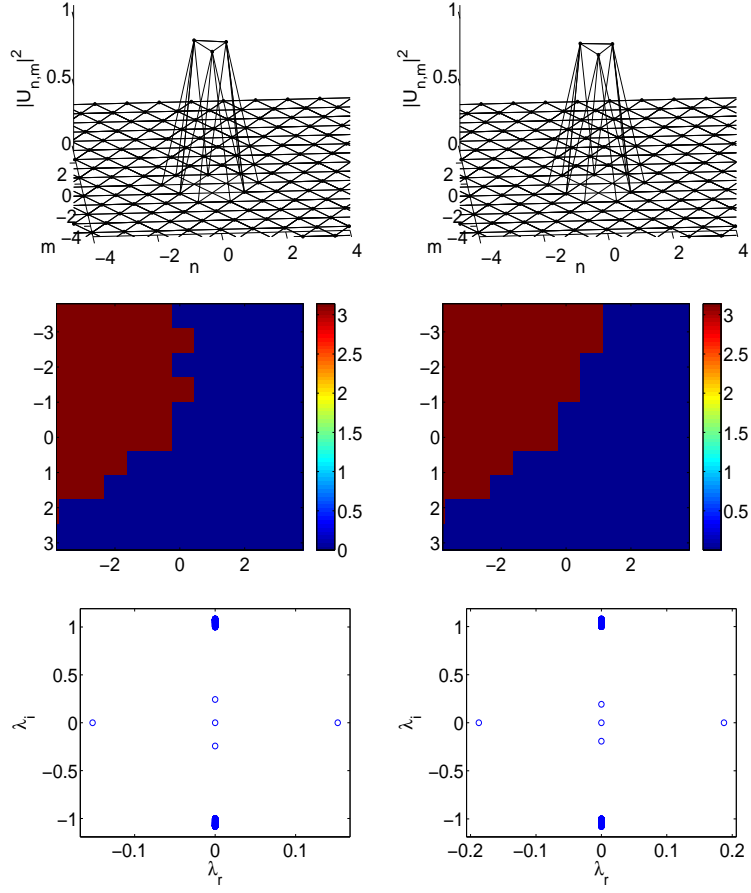
FIG. 3: Hexagonal three-site $[0, \pi, 0]$ configuration ($\varepsilon = 0.01$). The top row displays the modulus squared of the field with $\delta = 0.8$ (left column) and $\delta = 0$ (right column). The anisotropy is invoked between the node with phase π and one of the nodes with phase 0. At $\delta = 0$ the result is equivalent to an effective $[0, 0, \pi]$ configuration, along a line. Hence, in this case the instability is preserved for all values of δ.

FIG. 4: Hexagonal three-site $[0, 0, 0]$ configuration ($\varepsilon = 0.01$). The top row displays the modulus squared of the field with anisotropy 0.8 (left column) and 0 (right column). The configuration is found to be unstable for all values of δ, as also predicted theoretically.
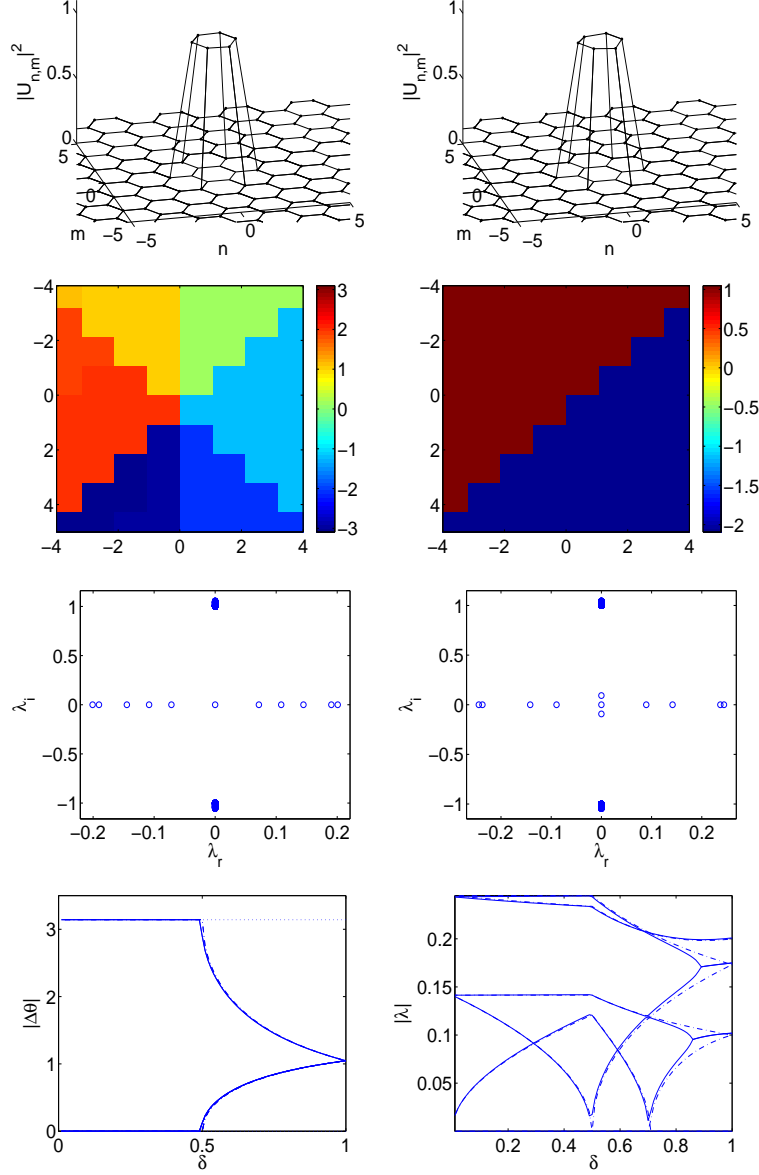
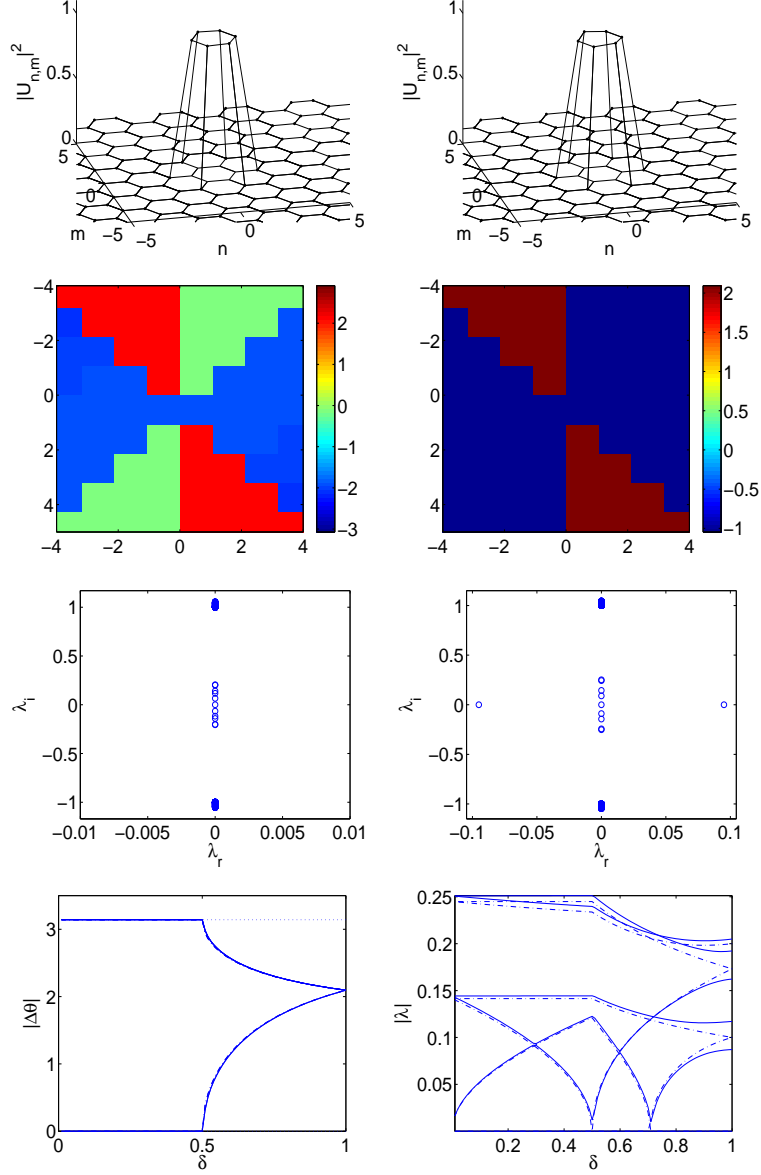FIG. 5: Honeycomb six-site charge 1 vortex i.e. the honeycomb $[0, \pi/3, 2\pi/3, \pi, 4\pi/3, 5\pi/3]$ configuration at the isotropic limit ($\varepsilon = 0.01$). The top row displays the modulus squared of the configuration corresponding to anisotropic parameter $\delta = 0.8$ (left panel) and $\delta = 0.3$ (right panel). The second row shows the phase portraits and the third row shows the spectral plane for the same values of the anisotropy, $\delta = 0.8$ (left), and $\delta = 0.3$ (right). In the last row the left panel shows the comparison between the theoretical (dash-dot lines) and numerical (solid lines) changes in the relative phases. The vortex collides at $\delta = 0.5$ with the $[\pi/3, \pi/3, \pi/3, -2\pi/3, -2\pi/3, -2\pi/3]$ configuration. At $\delta = 0$, for the present form of anisotropy, this is equivalent to the two configurations along a line, namely $[\pi/3, \pi/3, \pi/3]$ and $[-2\pi/3, -2\pi/3, -2\pi/3]$. The bottom right panel shows the comparison of the theoretical (dash-dot lines) versus numerical (solid lines) linear stability eigenvalues for $0 \leq \delta \leq 1$.

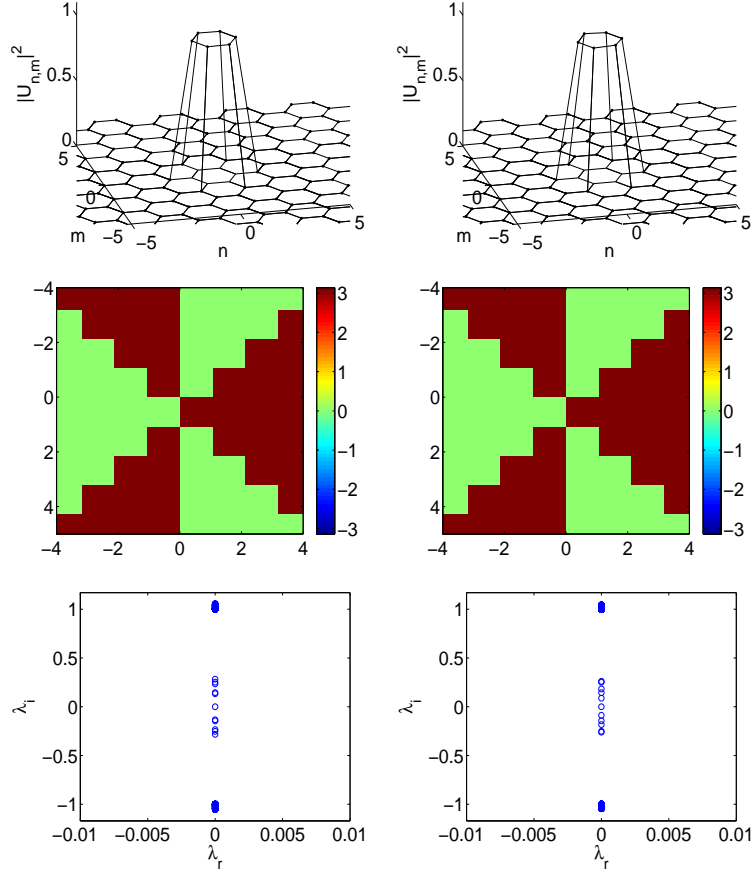FIG. 6: Honeycomb six-site charge 2 vortex i.e. the honeycomb $[0, 2\pi/3, 4\pi/3, 2\pi, 8\pi/3, 10\pi/3]$ configuration ($\varepsilon = 0.01$). The top row displays the modulus squared of the configuration corresponding to anisotropic parameter $\delta = 0.8$ (left panel) and $\delta = 0.3$ (right panel). The second row shows the phase portraits and the third row shows the spectral plane for the same values of the anisotropy, $\delta = 0.8$ (left), and $\delta = 0.3$ (right). In the last row the left panel shows the change in the relative phases. The charge 2 vortex collides at $\delta = 0.5$ with the $[-\pi/3, 2\pi/3, -\pi/3, -\pi/3, 2\pi/3, -\pi/3]$ configuration. The bottom right panel shows the theoretical (dash-dot lines) versus numerical (solid lines) comparisons of the linear stability eigenvalues for $0 \leq \delta \leq 1$.

15

FIG. 7: Honeycomb six-site out-of-phase configuration, i.e. honeycomb $[0, \pi, 0, \pi, 0, \pi]$ configuration ($\varepsilon = 0.01$). The top row displays the modulus squared of the field with $\delta = 0.8$ (left panel) and $\delta = 0.3$ (right panel). At $\delta = 0$ this is equivalent to the two configurations along a line of the form: $[0, \pi, 0]$ and $[\pi, 0, \pi]$. Hence it retains its stability throughout the interval $0 \leq \delta \leq 1$.
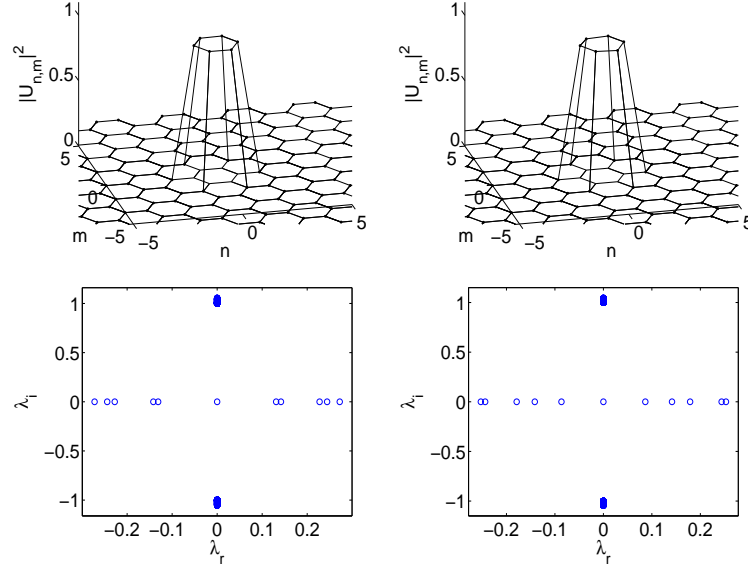
FIG. 8: Honeycomb six-site in-phase configuration, i.e. honeycomb $[0, 0, 0, 0, 0, 0]$ configuration ($\varepsilon = 0.01$) The top row displays the modulus squared of the field with anisotropy 0.8 (left column) and 0.3 (right column). As expected by the adjacency of sites with the same phase, the anisotropy cannot prevent this configuration from being highly unstable.
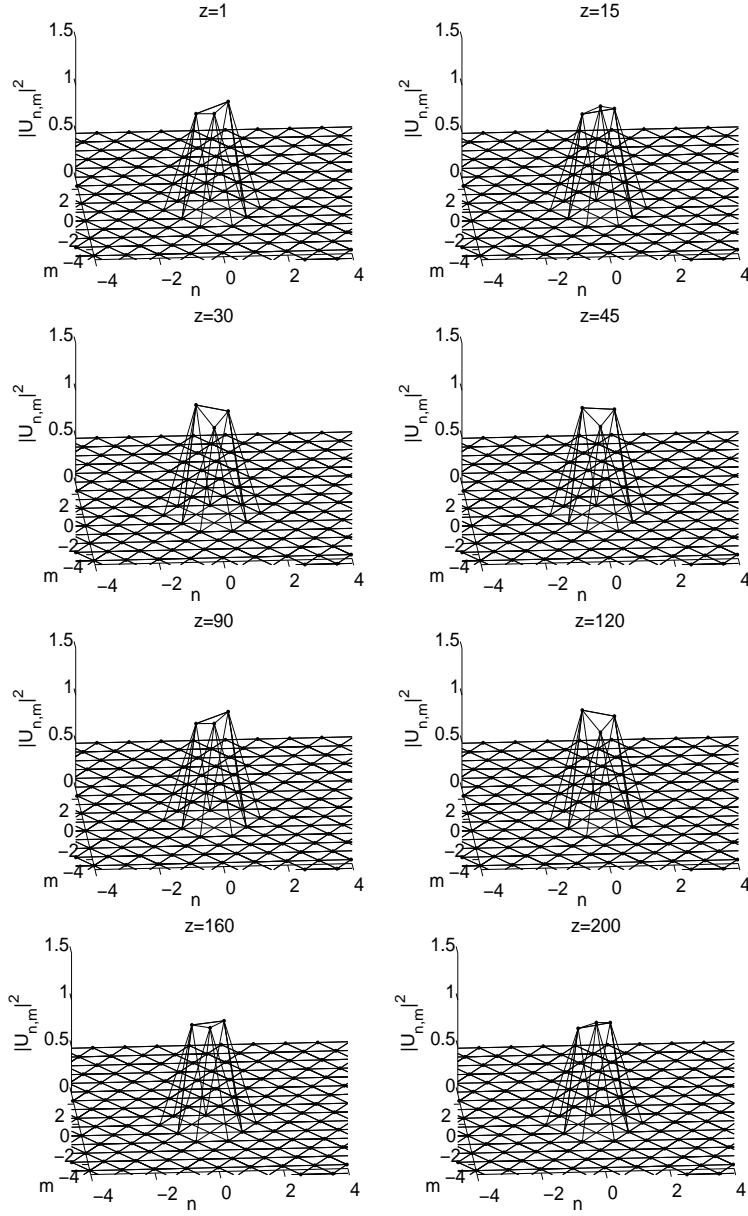
FIG. 9: RK4 results from the hexagonal three-site $[0, \pi, 0]$ with anisotropy between the sites with phase 0 at $\delta = 0.80$, $C = 0.01$ at $z = 1, 15, 30, 45, 90, 120, 160, 200$. The formation of a breathing pattern is clearly observed.
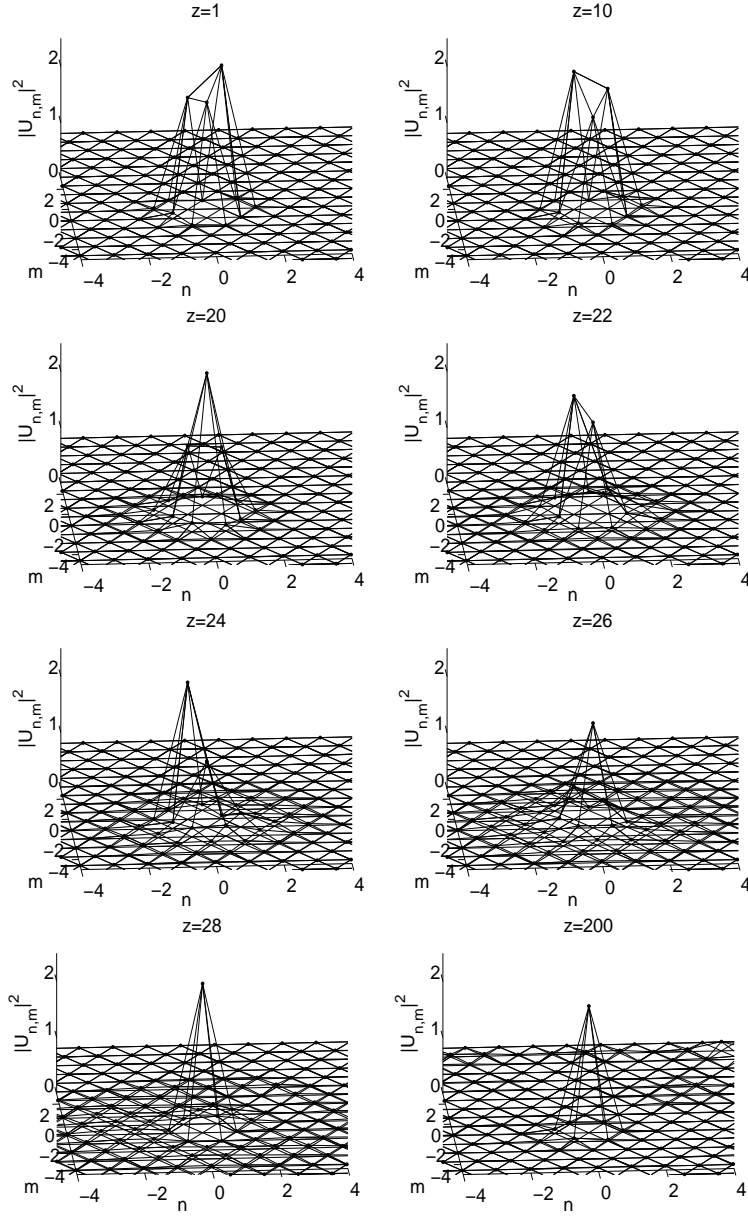
FIG. 10: RK4 results from the hexagonal three-site $[0, \pi, 0]$ with anisotropy between the sites with phase 0 at $\delta = 0.80$, $\varepsilon = 0.2$ at $z = 1, 10, 20, 22, 24, 26, 28, 200$. The emergence of a localized state centered on a single site is clearly evident.
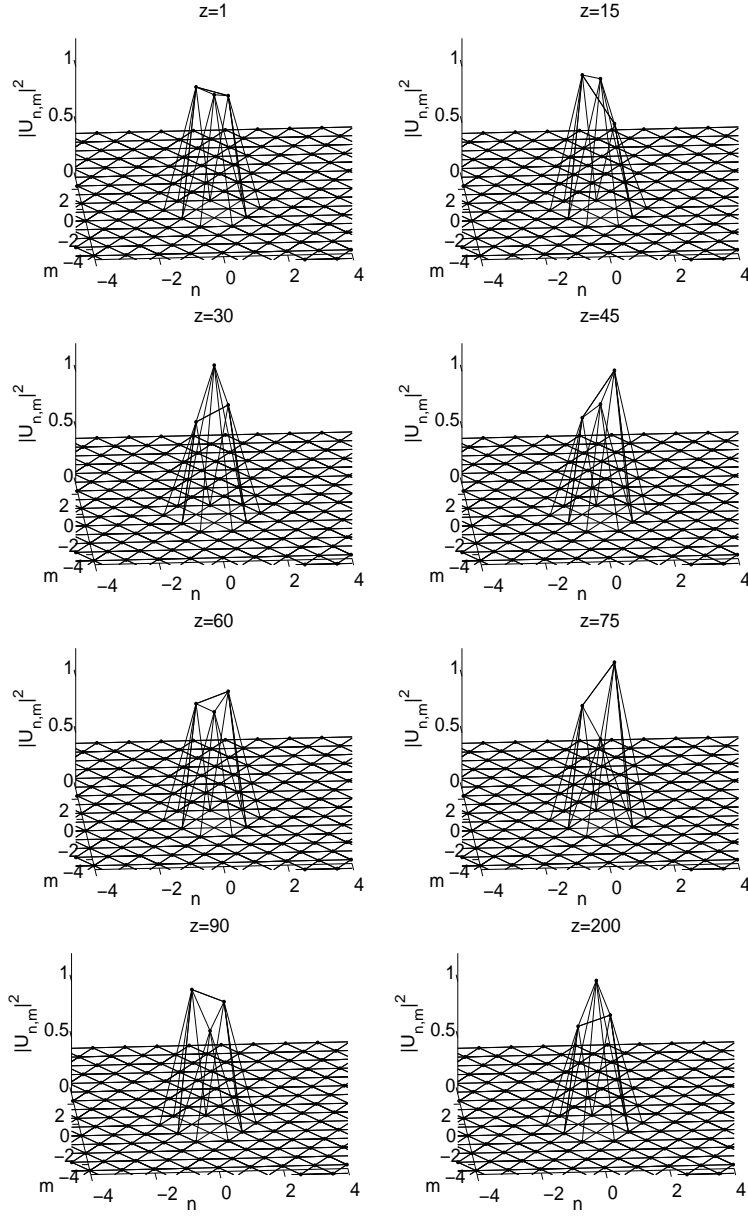
FIG. 11: RK4 results from the hexagonal three-site $[0, 0, 0]$ at $\delta = 0.80$, $\varepsilon = 0.01$ at $z = 1, 15, 30, 45, 60, 75, 90, 200$.
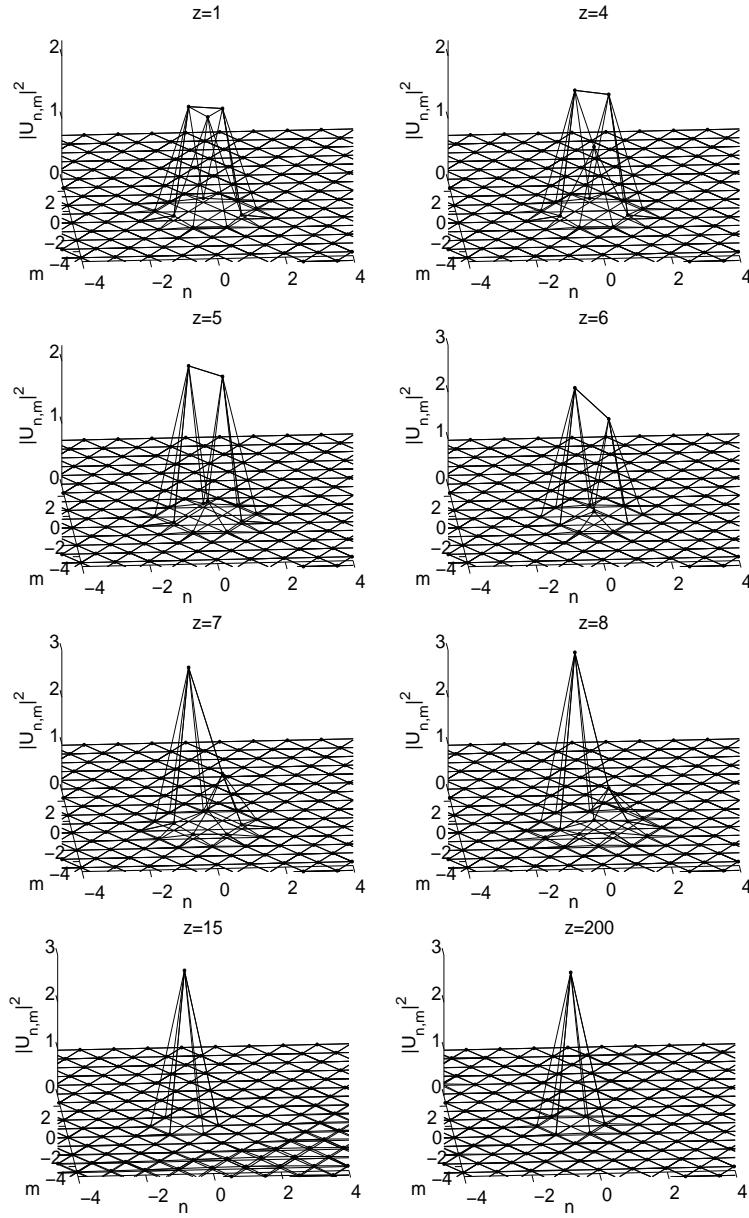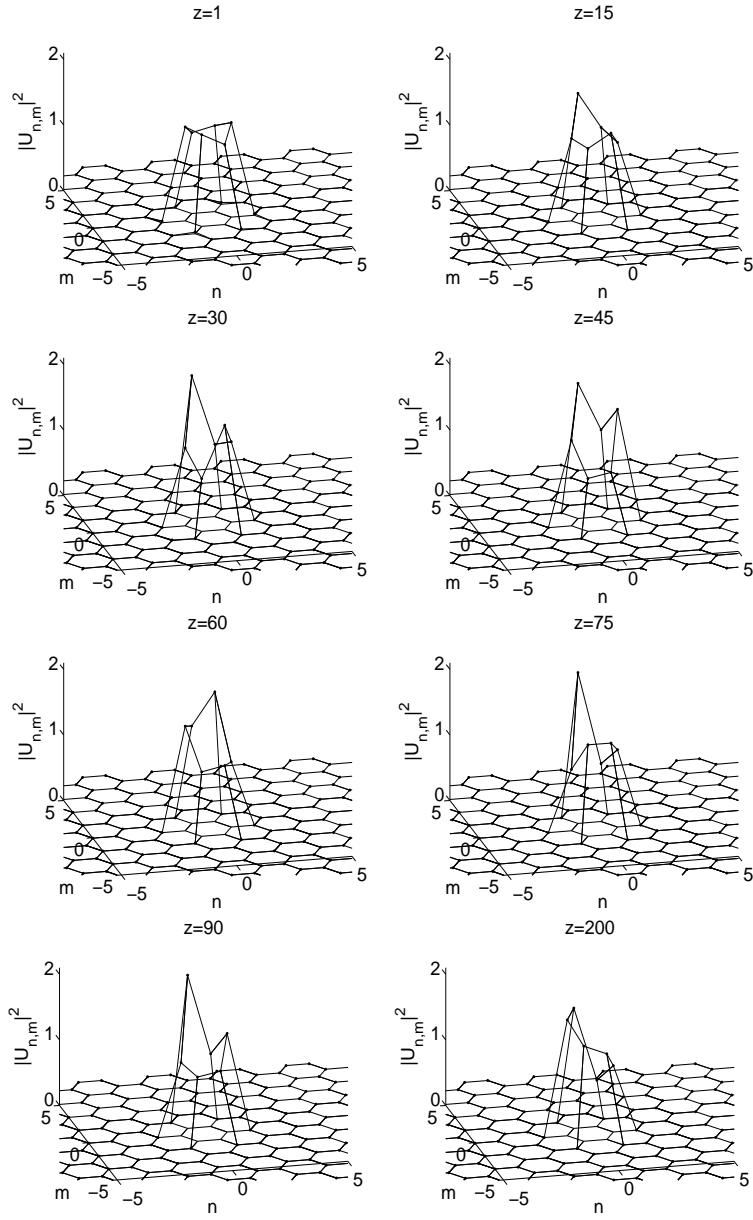
FIG. 12: RK4 results from the hexagonal three-site $[0,0,0]$ at $\delta = 0.80$, $\varepsilon = 0.2$ at $z = 1, 4, 5, 6, 7, 8, 15, 200$.

FIG. 13: RK4 results from the six site honeycomb charge 1 vortex at $\delta = 0.80$, $\varepsilon = 0.2$ at $z = 1, 15, 30, 45, 60, 90, 200$. A multi-site breather emerges with an associated repartitioning of the norm of the solution.
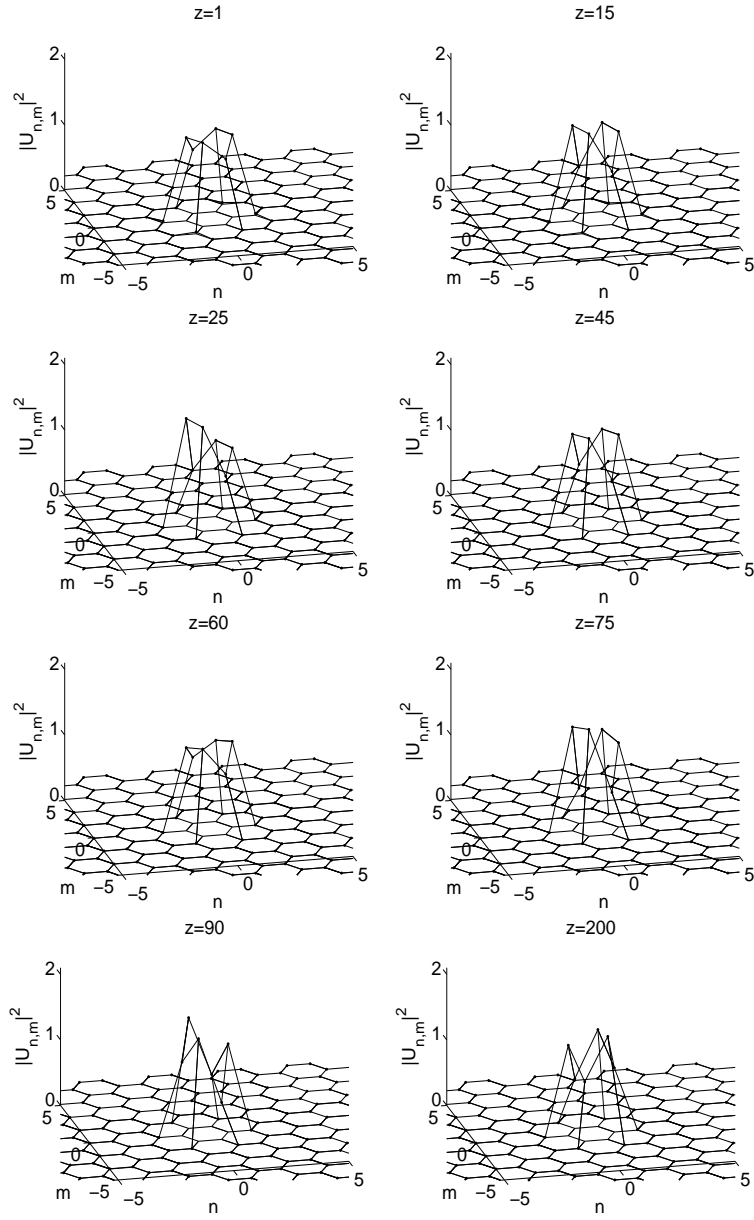
FIG. 14: Similar to the above case, i.e., RK4 results from the six site honeycomb charge 1 vortex at $\delta = 0.20$, $C = 0.2$ at $z = 1, 15, 25, 45, 60, 90, 200$.
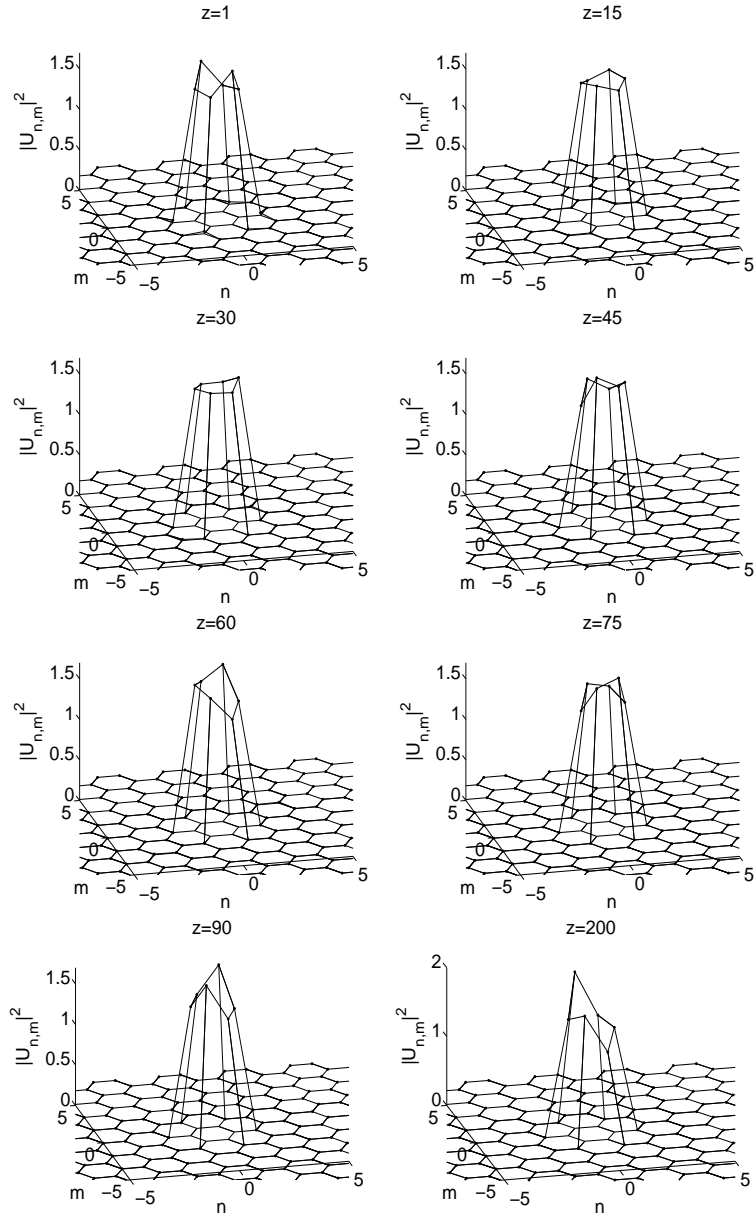
FIG. 15: RK4 results from the six site charge-2 vortex at $\delta = 0.60$, $\varepsilon = 0.2$ at $z = 1, 15, 25, 45, 60, 90, 200$. A complex multi-site breathing pattern results from the instability.
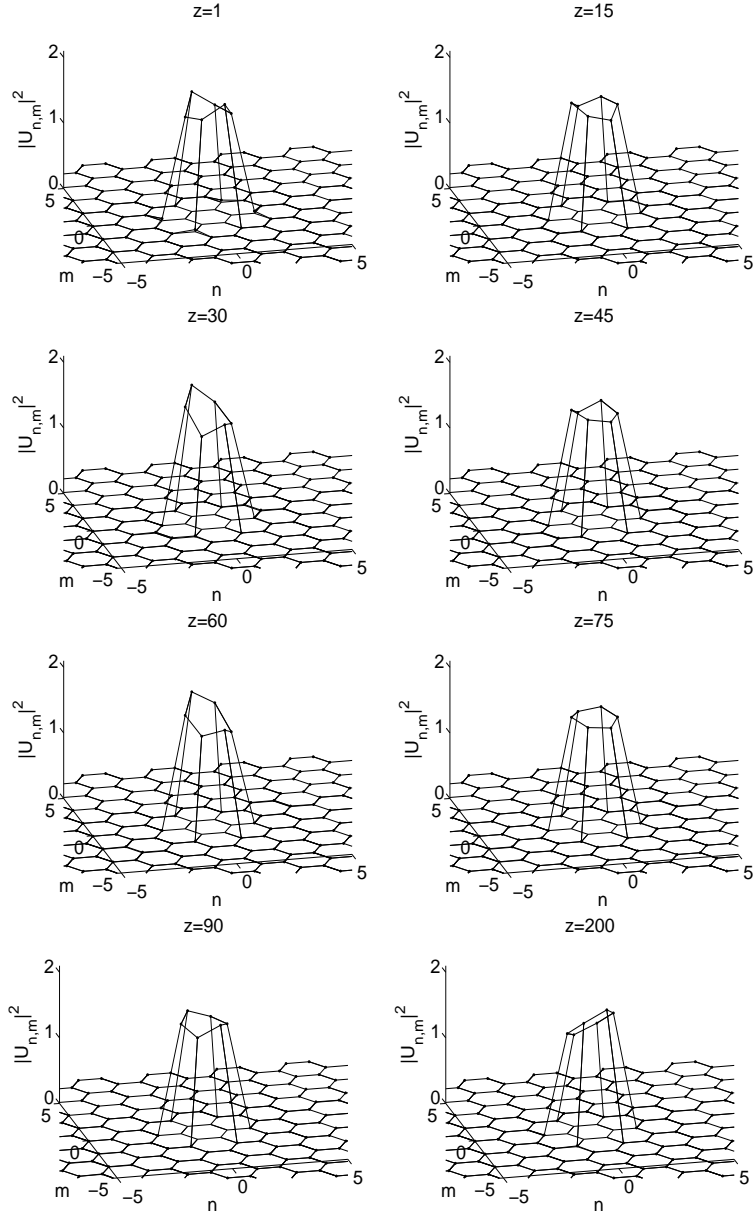
FIG. 16: RK4 results from the six site waveform $[0, 0 + \pi, 0, 0, 0 + \pi, 0]$ (resulting from the bifurcation of a charge-2 vortex) at $\delta = 0.20$, $\varepsilon = 0.2$ at $z = 1, 15, 25, 45, 60, 90, 200$.
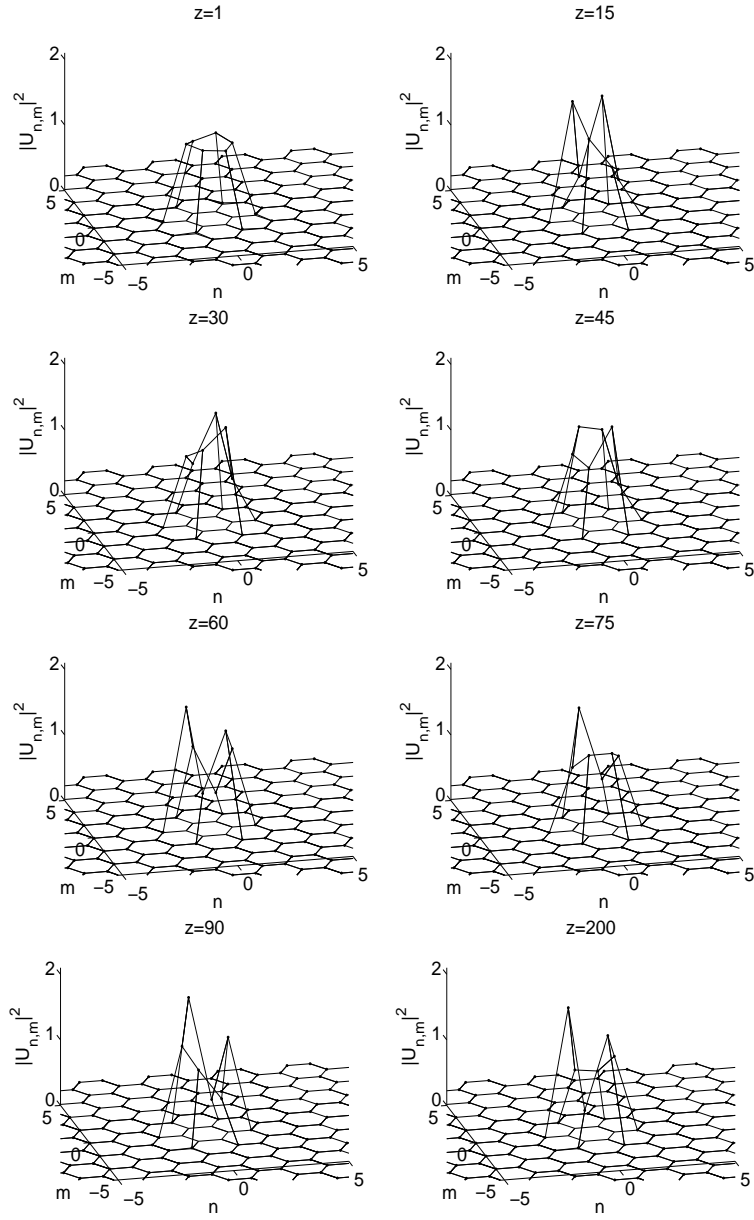
FIG. 17: RK4 results from the honeycomb six-site $[0,0,0,0,0,0]$ configuration at $\delta = 0.80$, $C = 0.2$ at $z = 1, 15, 25, 45, 60, 90, 200$. A state with fewer dominant sites appears to emerge from the instability dynamics.

[1] F. Lederer, G.I. Stegeman, D.N. Christodoulides, G. Assanto, M. Segev, Y. Silberberg, Phys. Rev. **463**, 1 (2008).

[2] O. Morsch and M. Oberthaler, Rev. Mod. Phys. **78**, 179 (2006).

[3] D. Christodoulides, F. Lederer and Y. Silberberg, Nature **424**, 817 (2003);

[4] J.W. Fleischer, G. Bartal, O. Cohen, T. Schwartz, O. Manela, B. Freedman, H. Buljan, N.K. Efremidis, Opt. Express **13**, 1780 (2005).

[5] V.A. Brazhnyi, V.V. Konotop, Mod. Phys. Lett. B **18**, 627 (2004).

[6] I. Bloch, J. Dalibard, W. Zwerger, Rev. Mod. Phys. **80**, 885 (2008).

[7] K.J.H. Law, P.G. Kevrekidis, V. Koukouloyannis, I. Kourakis, D.J. Frantzeskakis, and A.R. Bishop, Physical Review E **78**, 066610 (2008).

[8] B. Terhalle, T. Richter, K.J.H Law, D.G. Göries, P. Rose, T.J. Alexander, P.G. Kevrekidis, A.S. Desyatnikov, W. Krolikowski, F. Kaiser, C. Denz, Y.S. Kivshar, Physical Review A **79**, 043821 (2009).

[9] S. Liu, Y. Hu, P. Zhang, X. Gan, C. Lou, D. Song, J. Zhao, J. Xu and Z. Chen, Appl. Phys. Lett. **100**, 061907 (2012).

[10] S. Liu, Y. Hu, P. Zhang, X. Gan, C. Lou, D. Song, J. Zhao, J. Xu and Z. Chen, Opt. Lett. **37**, 2184 (2012).

[11] M. Rechtsman, Y. Plotnik, J.M. Zeuner, D. Song, Z. Chen, A. Szameit, M. Segev, Phys. Rev. Lett. **111**, 103901 (2013).

[12] Y. Plotnik, M. Rechtsman, D. Song, M. Heinrich, J.M. Zeuner, S. Nolte, Y. Lumer, N. Malkova, A. Szameit, Z. Chen, M. Segev, Nature Mat. **13**, 57 (2014).

[13] D. Song, V. Paltoglou, S. Liu, Y. Zhu, D. Gallardo, L. Tang, J. Xu, M. Ablowitz, N.K. Efremidis and Z. Chen, Nat. Comm. **6**, 6272 (2015).

[14] C. Becker, P. Soltan-Panahi, J. Kronjager, S. Doscher, K. Bongs, K. Sengstock, New J. Phys. **12**, 065025 (2010).

[15] P. Soltan-Panahi, J. Struck, P. Haue, A. Bick, W. Plenkers, G. Meineke, P. Windpassinger, M. Lewenstein, K. Sengstock, Nature Phys. **7**, 434 (2011).

[16] K. J. H. Law, A. Saxena, P. G. Kevrekidis, and A. R. Bishop, Phys. Rev. A **79**, 053818 (2009).

[17] R.A. Vicencio M. Johansson, Phys. Rev A **87**, 061803(R) (2013).

[18] P.G. Kevrekidis, *The discrete nonlinear Schrödinger equation: Mathematical Analysis, Numerical Computation and Physical Perspectives*, Springer-Verlag (Heidelberg, 2009).

[19] D.E. Pelinovsky, P.G. Kevrekidis, and D.J. Frantzeskakis, Physica D **212**, 1 (2005).

[20] R.S. MacKay and S. Aubry, Nonlinearity **7**, 1623 (1994).

[21] D.E. Pelinovsky, P.G Kevrekidis, and D.J. Frantzeskakis, Physica D **212**, 20 (2005).